

# Elucidating the origin of heterogeneous anomalous diffusion in the cytoplasm of mammalian cells

Adal Sabri<sup>1</sup>, Xinran Xu<sup>2</sup>, Diego Krapf<sup>2,3,\*</sup>, and Matthias Weiss<sup>1,\*</sup>

<sup>1</sup>*Experimental Physics I, University of Bayreuth, D-95440 Bayreuth, Germany*

<sup>2</sup>*Dept. of Electrical and Computer Engineering, and <sup>3</sup>School of Biomedical Engineering, Colorado State University, Fort Collins, CO 80523, USA*

Diffusion of tracer particles in the cytoplasm of mammalian cells is often anomalous with a marked heterogeneity even within individual particle trajectories. Despite considerable efforts, the mechanisms behind these observations have remained largely elusive. To tackle this problem, we performed extensive single-particle tracking experiments on quantum dots in the cytoplasm of living mammalian cells at varying conditions. Analyses of the trajectories reveal a strong, microtubule-dependent subdiffusion with antipersistent increments and a substantial heterogeneity. Furthermore, particles stochastically switch between different mobility states, most likely due to transient associations with the cytoskeleton-shaken endoplasmic reticulum network. Comparison to simulations highlight that all experimental observations can be fully described by an intermittent fractional Brownian motion, alternating between two states of different mobility.

The cytoplasm of mammalian cells is a complex aqueous environment, crowded with large amounts of macromolecules [1, 2] and a multitude of membrane-enveloped organelles of largely varying sizes. Diffusion of supposedly inert tracer particles in the cytoplasm of living cells has frequently been reported to be anomalous with a sub-linear scaling of the mean square displacement (MSD),  $\langle r^2(\tau) \rangle \sim t^\alpha$  ( $\alpha < 1$ ) on spatio-temporal scales below a few micrometers and several seconds [3–5]. The emergence of subdiffusive motion appears in many cases to be consistent with a stochastic process of the fractional Brownian motion (FBM) type [6–8], i.e. a self-similar Gaussian process with stationary increments whose features are determined by the Hurst coefficient  $H = \alpha/2$  [9]. FBM dynamics is subdiffusive for  $0 < H < 1/2$  and trajectories are characterized by antipersistent, i.e. anticorrelated, increments. A plausible interpretation for such antipersistent memory effects is a viscoelastic environment [10–15] with a complex shear modulus that scales as  $G(\omega) \sim \omega^\alpha$ , where the elastic and the viscous parts are responsible for the FBM memory and for energy dissipation, respectively.

Subdiffusion has long been recognized to emerge in solutions crowded with macromolecules, with an anomaly exponent  $\alpha$  that decreases with crowder concentration [16, 17]. However, the value of  $\alpha$  is often observed to be considerably lower in the cytoplasm than in similarly crowded artificially fluids, e.g.  $\alpha \approx 0.6$  [10, 18] versus  $\alpha \approx 0.8$  [11, 14]. Therefore, it is currently understood that subdiffusion in the cytoplasm may not be caused solely by macromolecular crowding but also relies on additional mechanisms. As of yet, no general agreement exists for a physical model that can reliably describe cytoplasmic subdiffusion in detail. Further, subdiffusion is not universal but depends on tracer size, e.g. for particles in reconstituted entangled actin filament networks, where  $\alpha$  can be continuously tuned between zero and unity as a function of particle radius and average mesh size [19].

Beyond such caging effects, it has also been proposed that non-inert crowders may strongly alter the dynamics of cytoplasmic particles [20, 21]. Extensive Monte Carlo simulations have supported this hypothesis [22]. More recently, also experimental support has been obtained via single-particle tracking (SPT) on surface-modified tracer particles in the cytoplasm of HeLa cells: The emergence of subdiffusion and the value of  $\alpha$  was shown to depend both on particle size and non-specific interactions to the cytoplasmic interior [18]. Yet, the identity of the cytoplasmic binding partners that enforce the emergence of subdiffusive motion has remained elusive. Potential candidates include the cytoskeleton and organelles, e.g. the endoplasmic reticulum (ER) network that pervades the cytoplasm [23].

Further, local variations in complex media are noticeable in the motion of particles therein: (Sub)diffusion in cellular fluids has been observed to be heterogeneous even within individual trajectories [24–26], suggesting heterogeneous diffusion processes [27] or spatiotemporal variations of transport coefficients [28–30]. Despite the elegance of these theoretical models, it remains an open question how a distribution of apparent diffusivities emerges in the first place. A potential source might be the ambient active noise in the cytoplasm, i.e. the chemically induced rattling and shaking of the environment due to the non-equilibrium action of molecular motors and cytoskeletal filaments. In fact, breaking down cytoskeletal filaments alters the subdiffusive motion of organelle structures in mammalian cells [31, 32] and also compromises the superdiffusive motion of beads in migrating amoebae [26]. Taken together, it is currently neither clear (i) which mechanism regulates the value of the anomaly exponent  $\alpha$  in the cytoplasm nor (ii) how one should picture the emergence of heterogeneous subdiffusion due to non-specific interactions in an actively driven environment.

Here, we address these points by extensive SPT ex-

periments on individual quantum dots loaded into the cytoplasm of living mammalian cells. In particular, we quantify the particles' motion in the cytoplasm of untreated cells and in cells where the actin or microtubule cytoskeleton, or the ER has been disrupted. In all cases, a distinct and heterogeneous subdiffusion of tracers is seen. The subdiffusion effects become more pronounced when microtubules are broken down. Detailed analyses reveal that particles switch stochastically between at least two mobility states, irrespective of the cytoskeleton integrity, but clearly dependent on the presence of an intact ER network. This evidence suggests non-specific binding of tracers to the ER network, and hence an indirect coupling to active microtubule-based processes, to be responsible for the observed heterogeneous subdiffusion in the cytoplasm. Our experimental data are well described by an intermittent FBM model that switches stochastically between a higher and lower mobility, supposedly representing free motion in the cytosol and co-movement with ER segments.

To explore the heterogeneous subdiffusion in the cytoplasm of mammalian cells, we performed extensive SPT on quantum dots that had been introduced into the cytoplasm of cultured HeLa cells by bead loading [33, 34]. Measurements were performed with a sampling time of  $\Delta t = 100$  ms, and quantum dot trajectories were first evaluated in terms of their time-averaged MSD (TA-MSD) using  $N = 100$  or  $N = 500$  positions,

$$\langle r^2(\tau) \rangle_t = \frac{1}{N-k} \sum_{i=1}^{N-k} [\mathbf{r}((i+k)\Delta t) - \mathbf{r}(i\Delta t)]^2. \quad (1)$$

Following previous reports [18, 35, 36], individual TA-MSDs were fitted with a simple power law  $\langle r^2(\tau) \rangle_t = K_\alpha \tau^\alpha$  in the range  $\Delta t \leq \tau \leq 10\Delta t$  to extract the anomaly exponent  $\alpha$  and the generalized diffusion coefficient  $K_\alpha$ . The resulting probability density function (PDF) of anomaly exponents,  $p(\alpha)$ , showed considerable trajectory-to-trajectory fluctuations around a mean  $\langle \alpha \rangle \approx 0.57$  (Fig. 1 and Fig. S1a in [34]) that slightly depends on the trajectory length  $N$  (Table I). Control experiments in highly viscous artificial solutions yielded  $\langle \alpha \rangle \approx 1$  (Sect. C and Fig. S2f,g in [34]).

To probe a potential perturbation of the power-law scaling due to static and dynamic localization errors [37], and to validate the significance of the mean exponent  $\langle \alpha \rangle$ , we exploited a bootstrapping approach [34]: From the whole set of calculated TA-MSDs we drew randomly a non-exhaustive ensemble of 100 curves, averaged these geometrically, and used again a simple power-law fit to extract the scaling exponent  $\alpha$  of the resulting ensemble-averaged TA-MSD. Repeating this approach  $M = 200$  times, we noted that none of the ensemble-averaged TA-MSDs showed a significant offset in the limit  $\tau \rightarrow 0$  (Sect. E and Fig. S2a-d in [34]). Hence, positive and negative contributions from static and dynamic localiza-

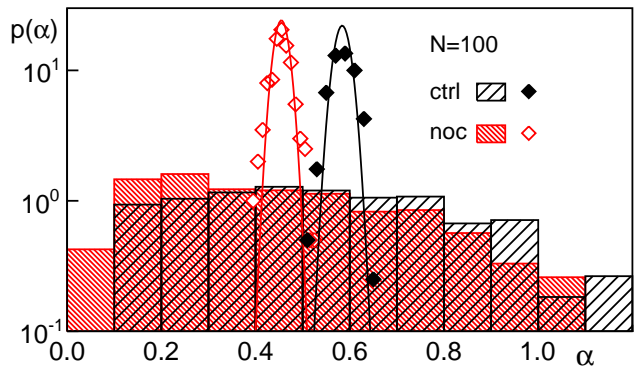


FIG. 1: The PDF of anomaly exponents  $\alpha$ , obtained from individual TA-MSDs ( $N = 100$ ), shows a broad variation around a mean  $\langle \alpha \rangle = 0.59$  in untreated cells (black histogram). Nocodazole-treated cells have a similarly broad PDF (red histogram) with a significantly lower mean (cf. Table I). Similar results are found for longer trajectories (Fig. S1a in [34]). Using a bootstrapping approach with geometric averaging (diamonds; full lines are Gaussian fits) resulted in narrower PDFs with the same mean,  $\langle \alpha \rangle$ .

	untreat.	noc	cyto D	lat A
TA-MSDs	0.59 (0.55)	0.46 (0.36)	0.58 (0.54)	0.62 (0.58)
b.tr. geom.	0.58 (0.55)	0.46 (0.36)	0.58 (0.54)	0.61 (0.57)
b.tr. arith.	0.79 (0.60)	0.66 (0.43)	0.82 (0.73)	0.86 (0.76)

TABLE I: Mean anomaly exponents  $\langle \alpha \rangle$  for trajectories of length  $N = 100$  ( $N = 500$ ) in untreated cells and after application of nocodazole, cytochalasin D, or latrunculin A. Standard errors were in all cases smaller than 0.02.

tion errors appear to cancel each other in our data and therefore fitting with a simple power law gives meaningful results for  $\alpha$ .

The PDF of  $\alpha$  values obtained with the bootstrapping approach (Fig. 1) was very narrow with a mean  $\langle \alpha \rangle$  that matched the respective value found before via individual TA-MSDs (Table I). Geometric averaging of TA-MSDs boils down to an arithmetic averaging of individual  $\alpha$  values (but not of  $K_\alpha$ ). Thus, the narrow width of  $p(\alpha)$  after bootstrapping is determined by  $\sigma/\sqrt{M}$ , where  $\sigma$  is the standard deviation of  $\alpha$  derived from individual TA-MSDs. Analyzing TA-MSDs with a recently introduced and validated resampling algorithm [38] confirmed the values for  $\langle \alpha \rangle$  [34]. An arithmetic instead of a geometric averaging of TA-MSDs lead to an overestimation of the mean scaling exponent (Table I and Fig. S1b in [34]).

Being interested in how cytoplasmic diffusion is affected by the cytoskeleton, we applied either nocodazole to break down microtubules, or cytochalasin D or latrunculin A to disrupt actin filaments. Disrupting microtubules changed the diffusion anomaly substantially (Fig. 1 and Table I) whereas disrupting actin networks

had no significant effect (Table I). Transport coefficients  $K_\alpha$  showed a higher sensitivity to microtubule disruption and also a stronger dependence on trajectory length (Fig. S1c in [34]). Similar to previous observations on the dynamics of the ER [32], the effect of nocodazole on  $K_\alpha$  was not particularly strong for short trajectories. For longer trajectories, however, a marked shift to smaller transport coefficients was visible upon microtubule disruption. This puts up a caveat that longer trajectories may represent a distinct subset of the acquired data, e.g. a lower mobility facilitating the tracking, but it also indicates that microtubule-associated processes significantly contribute to the diffusion anomaly in untreated cells beyond a change in the scaling of MSDs.

Going beyond the MSD, we analyzed the ensemble average of the velocity autocorrelation function (VACF),

$$C_v(\tau) = \langle \mathbf{v}(t)\mathbf{v}(t+\tau) \rangle_{t,E} \quad (2)$$

that is highly sensitive to the nature of unconfined anomalous diffusion processes [39, 40]. Here,  $\mathbf{v}(t) = [\mathbf{r}(t+\delta t) - \mathbf{r}(t)]/\delta t$  is the velocity at time  $t$ , given via the increments in a period  $\delta t$ . Varying  $\delta t = k\Delta t$  in multiples of the sampling time  $\Delta t$ , the VACFs showed in all cases a pronounced negative peak for  $\tau = \delta t$  as expected for antipersistent random walks. By rescaling the times as  $\xi = \tau/\delta t$ , all VACF traces collapse to a single master curve that agrees with the analytical predictions for FBM (Fig. 2 and Fig. S3a in [34]), namely

$$C_v(\xi) = \{(\xi+1)^\alpha + |\xi-1|^\alpha - 2\xi^\alpha\} / 2, \quad (3)$$

with  $\alpha$  being set to the value  $\langle \alpha \rangle$  found with the bootstrapping protocol (Table I). We emphasize the exceptional agreement of the experimental data with Eq. (3) without any fitting parameters since other antipersistent random walk data, e.g. from membrane proteins, can deviate significantly from the FBM prediction (see Fig. S3b [34] for an example).

Next we inspected the PDF of the normalized increments  $\chi$  within a time lag  $\delta t$  [25], i.e. time series  $\Delta x_i = x_{i+k} - x_i$  and  $\Delta y_i = y_{i+k} - y_i$  were calculated and normalized by their individual root-mean-square step length. Since no systematic differences were observed between  $x$ - and  $y$ -directions, all normalized increments were combined into a single set of  $\chi$ . For a homogeneous FBM, a Gaussian PDF  $p(\chi)$  is expected for all  $\delta t$ . Yet, for small  $\delta t$  our data showed significant deviations from a Gaussian in the tails of the distribution (Fig. 3a and Fig. S4a in [34]). This suggests that individual trajectories are heterogeneous, i.e. the particle mobility changes within the trajectory. For  $\delta t = 10\Delta t$ , this heterogeneity subsides, collapsing the increment statistics to the anticipated Gaussian (Fig. S4b in [34]).

To directly probe switching between different mobilities, we analyzed the local convex hull (LCH) of individual trajectories [34, 41]: After normalizing the trajectories

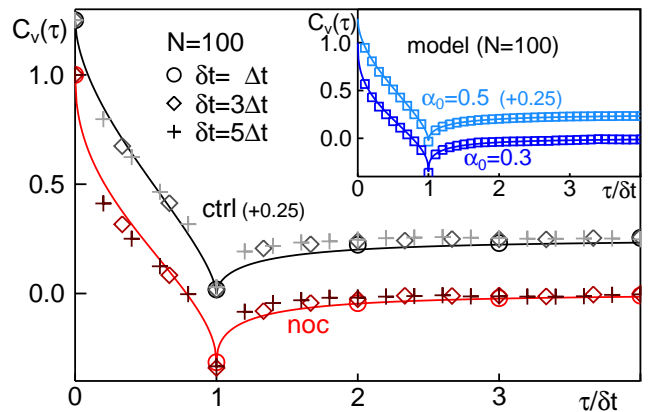


FIG. 2: Rescaled normalized VACFs [Eq. (2)] of all experimental trajectories with  $N = 100$  at different  $\delta t$  agree with the analytical prediction for FBM (full lines, Eq. (3)), without treatment (grey symbols) and after nocodazole-treatment (red symbols). For better visibility, untreated cell data have been shifted upwards. No significant differences are seen for longer trajectories (Fig. S3a in [34]). An estimate of  $\langle \alpha \rangle$  can be directly obtained from the VACF minimum,  $C_v(\xi = 1) = 2^{\alpha-1} - 1$ . VACF minima for untreated and nocodazole-treated cells yield  $\alpha = 0.58 \pm 0.01$  and  $\alpha = 0.38 \pm 0.02$ , respectively, in favorable agreement with our MSD results. Inset: VACFs of simulated intermittent FBM trajectories ( $N = 100$ , anomaly parameter  $\alpha_0$ ) also agree with Eq. (3) (full lines).

by their root-mean-square step length, we determined for each trajectory the largest diameter  $S_d(t)$  of the LCH for positions visited in the period  $[t-2\Delta, t+2\Delta]$  (see Fig. 3b for illustration). Using the mean  $\mu$  and standard deviation  $\sigma$  of all  $S_d$  values for a given cell condition, we defined a threshold  $\mu + \sigma$  and rated particles to be in a more mobile state for  $S_d(t) \geq \mu + \sigma$  (see also Fig. S6 in [34]). As a result, we observed a frequent switching between a lower- and a higher-mobility state (named 'on' and 'off', respectively) with markedly larger mean residence times  $\tau$  in the low-mobility state, irrespective of any treatment (see PDFs  $p(\tau)$  in Fig. 3c). Employing a threshold  $\mu + \sigma$ , all trajectories exhibit switching behavior. However, upon increasing the threshold, a growing fraction of trajectories does not display any switching (Fig. 3d) while no substantial difference is seen in the mean residence times (see Fig. S6c in [34]). Hence, the LCH analysis confirms the existence of at least two mobility states for untreated and nocodazole-treated cells. Additional support for a switching behavior is given by the autocorrelation function of squared increments,  $G(\tau)$ , which shows a long-lasting decay (Sect. G and Fig. S5 in [34]).

Based on these results and previous observations on the cytoskeleton-dependent anomalous dynamics of ER junctions [32], we hypothesized that particle interactions with the ubiquitous ER network are key for the observed switching of mobilities. We therefore repeated tracking

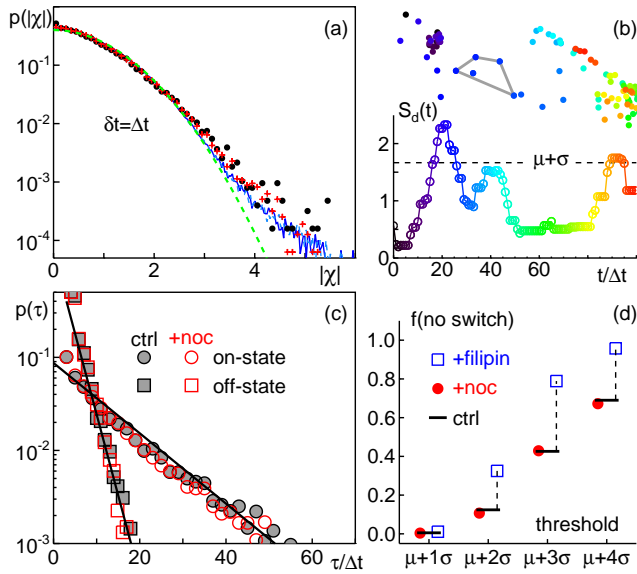


FIG. 3: (a) PDFs of normalized increments (time lag  $\delta t = \Delta t$ , shown here as moduli,  $|\chi|$ ) follow the anticipated Gaussian (green dashed line) for small  $|\chi|$  but show significant deviations for  $|\chi| > 3.5$ , indicating a heterogeneous process (black circles and red crosses: untreated and nocodazole-treated cells). These data are in excellent agreement with simulations of an intermittent FBM model ( $\alpha_0 = 0.5$  and  $\alpha_0 = 0.3$ : coinciding light and dark blue lines). (b) Representative trajectory (color-coded successive positions) with a local convex hull (LCH) at  $t = 28\Delta t$  highlighted in grey. The corresponding time series of largest LCH diameters,  $S_d(t)$ , shows considerable fluctuations. Values  $S_d(t) \geq \mu + \sigma$  (dashed horizontal line) are rated to be in the more mobile 'off'-state. (c) Residence times in the low- and high-mobility state, extracted from individual trajectories (threshold  $\theta = \mu + \sigma$ ) feature exponential PDFs (full black lines) with a substantially longer mean residence time in the 'on'-state. No substantial differences are seen for nocodazole-treatment or when choosing a threshold  $\theta = \mu + 2\sigma$  (Fig. S6c in [34]). (d) The fraction of trajectories without any switching rises when successively increasing the threshold value to  $\theta = \mu + 4\sigma$ . No significant differences are seen between untreated (black horizontal stripes) and nocodazole-treated cells (filled red circles). In contrast, trajectories from filipin-treated cells (open blue squares) feature a much stronger increase (highlighted by dashed lines), indicating that ER structures are required for the mobility switching.

experiments in cells where the ER network had been fragmented either using the drug filipin [34, 42] or by an osmotic shock [34, 43] (see Fig. 4). We observed that a lack of ER tubules did not grossly alter the scaling exponent  $\langle \alpha \rangle \sim 0.6$ . Yet, the intermittent nature of the particle motion was markedly reduced as evidenced by the LCH analysis (Fig. 3d), i.e. trajectories with a switching of mobilities become more rapidly diminished when altering the threshold for  $S_d(t)$ . This indicates that association to and dissociation from ER tubules is involved in creating

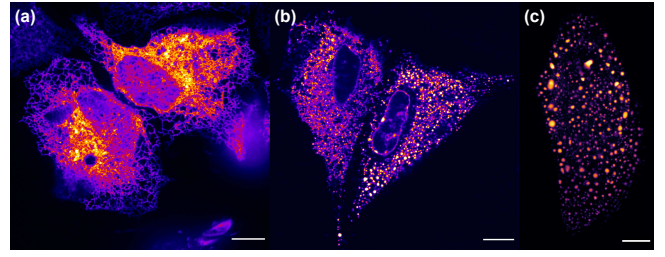


FIG. 4: Representative fluorescence images of the ER in (a) untreated, (b) filipin-treated, and (c) osmotically shocked cells. In line with previous reports [42, 43], the ER network of untreated cells is completely fragmented after filipin treatment or osmotic shock. Scale bars: 10  $\mu\text{m}$ .

the intermittent nature of the particles' diffusion.

Having observed a heterogeneous, intermittent, ER- and cytoskeleton-dependent subdiffusion of quantum dots in the cytoplasm, we used Occam's razor to formulate the simplest model that can capture our experimental data (see [34] for a discussion of more elaborate models). Taking all experimental constraints into account, we arrived at an intermittent FBM model: We modeled the dynamics of individual particles as FBM with fixed anomaly  $\alpha_0$  and a transport coefficient that randomly switches within each trajectory [34]. Particles were assumed to exist in 'on' and 'off' states with transport coefficients  $K_\alpha^{\text{on}} < K_\alpha^{\text{off}}$ , representing ER-tubule associated and free motion. Dichotomous switching between these states was modeled as a Markov process with transition rates  $k_{\text{on}}$  and  $k_{\text{off}}$ . In our simulations we kept these rates and the ratio  $s = K_\alpha^{\text{on}}/K_\alpha^{\text{off}}$  fixed, and chose  $\alpha_0 = 0.5$  ( $\alpha_0 = 0.3$ ) for untreated (nocodazole-treated) cells, in accordance with the previously reported anomaly values for ER junctions [32]. Despite the simplicity of this model, we observed a surprisingly good overlap with our experimental data when choosing  $s = 3.5$ ,  $k_{\text{on}} = 0.27 \text{ s}^{-1}$ , and  $k_{\text{off}} = 0.01 \text{ s}^{-1}$ : First, the mean anomaly of simulated realizations, extracted from TA-MSDs, was  $\langle \alpha \rangle = 0.55$  and  $\langle \alpha \rangle = 0.37$ , respectively, in agreement with experimental observations (Table I). The slightly larger value as compared to the imposed value  $\alpha_0$  is a consequence of the dichotomous switching that perturbs the pure FBM behavior. Second, when using the respective value  $\langle \alpha \rangle$ , the VACF showed the same agreement with Eq. (3) as the experimental data (insets of Fig. 2 and Fig. S3a in [34]). Third, the non-Gaussian shape of the increment  $\chi$  statistics for  $\delta t = \Delta t$  and a more Gaussian shape for  $\delta t = 10\Delta t$  are almost perfectly matched (Fig. 3a and Fig. S4 in [34]). Fourth, the shape of  $G(\tau)$  overlapped very well with the experimental data (Fig. S5 in [34]). Moreover, the PDFs of residence times in the 'on' and 'off' states were in favorable agreement with our experimental results (Sect. F in [34]). We therefore conclude that our minimal model is sufficient for reproducing the



- G. D. Reynolds, E. Laplantine, S. Y. Bednarek, S. L. Shorte, and K. W. Eliceiri, *Methods* **115**, 80 (2017).
- [47] K. Jaqaman, D. Loerke, M. Mettlen, H. Kuwata, S. Grinstein, S. L. Schmid, and G. Danuser, *Nat. Meth.* **5**, 695 (2008).
- [48] E. Kepten, I. Bronshtein, and Y. Garini, *Phys. Rev. E* **87**, 052713 (2013).
- [49] D. Arcizet, B. Meier, E. Sackmann, J. O. Rädler, and D. Heinrich, *Phys. Rev. Lett.* **101**, 248103 (2008).
- [50] G. Campagnola, K. Nepal, B. W. Schroder, O. B. Peersen, and D. Krapf, *Sci. Rep.* **5**, 17721 (2015).
- [51] M. G. Gervasi, X. Xu, B. Carbajal-Gonzalez, M. G. Buffone, P. E. Visconti, and D. Krapf, *J. Cell Sci.* **131**, jcs215897 (2018).
- [52] J. Cao, *Phys. Rev. E* **63**, 041101 (2001).
- [53] L. Stadler, K. Speckner, and M. Weiss, *Biophys. J.* **115**, 1552 (2018).
- [54] M. J. Metz, R. L. Pennock, D. Krapf, and S. T. Hentges, *Sci Rep* **9**, 7297 (2019).
- [55] J.-H. Jeon, A. V. Chechkin, and R. Metzler, *Phys. Chem. Chem. Phys.* **16**, 15811 (2014).
- [56] S. Sadegh, J. L. Higgins, P. C. Mannion, M. M. Tamkun, and D. Krapf, *Phys. Rev. X* **7**, 011031 (2017).
- [57] A. Lubelski, I. Sokolov, and J. Klafter, *Phys. Rev. Lett.* **100**, 250602 (2008).
- [58] Y. He, S. Burov, R. Metzler, and E. Barkai, *Phys. Rev. Lett.* **101**, 058101 (2008).